One-dimensional Dirac electrons on the surface of weak topological insulators

Alexander Lau,[1] Carmine Ortix,[1] and Jeroen van den Brink[1,2]
[1]*Institute for Theoretical Solid State Physics, IFW Dresden, 01171 Dresden, Germany*
[2]*Department of Physics, TU Dresden, 01062 Dresden, Germany*
(Received 16 October 2014; revised manuscript received 16 January 2015; published 11 February 2015)

We show that a class of weak three-dimensional topological insulators feature one-dimensional Dirac electrons on their surfaces. Their hallmark is a linelike energy dispersion along certain directions of the surface Brillouin zone. These one-dimensional Dirac line degeneracies are topologically protected by a symmetry that we refer to as *in-plane time-reversal invariance*. We show how this invariance leads to Dirac lines in the surface spectrum of stacked Kane-Mele systems and more general models for weak three-dimensional topological insulators.

DOI: 10.1103/PhysRevB.91.085106 PACS number(s): 73.20.−r, 72.25.−b, 73.43.−f, 85.75.−d

I. INTRODUCTION

The field of topological properties of matter is one of the most active areas in condensed matter physics [1–5]. In particular, topological insulators (TIs) have attracted a lot of attention in recent years due to their unique physical properties and potential applications [6,7]. In contrast to conventional insulators, TIs feature topologically robust gapless edge or surface states with a linear Dirac dispersion. Most interestingly, these so-called topological surface states are a direct physical consequence of the nontrivial topology of the bulk band structure and protected by time-reversal symmetry.

The number of inequivalent classes of TIs depends on the dimension of the systems under consideration [8,9]. In two dimensions, there is only one class that is characterized by a single topological invariant. Experimental realizations are, for instance, HgTe quantum well structures [10,11]. In three dimensions, TIs are described by a quadruple of topological invariants and their variety is, therefore, much larger. One then distinguishes between weak and strong TIs. The latter possess an odd number of Dirac-like surface states at the time-reversal invariant (TRI) momenta of the surface Brillouin zone (BZ). For this reason, they are stable against generic perturbations preserving time-reversal symmetry. On the contrary, weak TIs are unstable against translational-symmetry breaking perturbations, such as charge density waves, due to the presence of an even number of Dirac-like degeneracies in the surface band structure. Furthermore, they are topologically equivalent to a stack of layers of two-dimensional (2D) TIs. Both classes have been identified experimentally, including, for instance, the strong TIs $Bi_{1-x}Sb_x$ [10–12], Bi_2Te_3 [13], Bi_2Se_3 [14], as well as the recently found weak TI $Bi_{14}Rh_3I_9$ [15].

The topologically protected surface Kramers doublets found in three-dimensional (3D) TIs are usually referred to as Dirac points [9,16], since in their vicinity the dispersion of the surface states resembles that of a 2D Dirac electron [see Fig. 1(b)]. However, a recent experimental work by Gibson *et al.* [17] suggests that 3D TIs can also exhibit Dirac-like *line* degeneracies on their surfaces corresponding to effectively one-dimensional (1D) Dirac electrons. By angle-resolved photoemission spectroscopy, they established the presence of highly anisotropic surface states on the (113) surface of Ru_2Sn_3, which show an almost linelike dispersion along certain high-symmetry directions.

Thus far, 1D Dirac states have not been investigated in the context of 3D topological insulators. The first question that arises is whether and under what circumstances topological insulators can exhibit Dirac-like line degeneracies on their surface, and, secondly, whether they are protected by any kind of symmetry. In this paper, we establish that Dirac lines naturally occur in weak topological insulators during the transition from effectively two dimensions to three dimensions. Furthermore, these lines are topologically protected by a symmetry that we refer to as *in-plane time-reversal invariance*.

The paper is organized as follows. In Sec. II, we introduce the concept of in-plane time-reversal invariance, thereby showing how it leads to topologically protected Dirac lines on the surface of weak TIs. In Secs. III and IV, we will explicitly demonstrate how Dirac lines arise due to in-plane time-reversal invariance in two paradigmatic weak TI model Hamiltonians, namely stacked Kane-Mele systems [18,19], and the cubic Liu-Qi-Zhang model [16]. Finally, we will draw our conclusions in Sec. V.

II. IN-PLANE TIME-REVERSAL INVARIANCE

Let us consider a stack of arbitrary but identical 2D TIs where the stacking direction is, without loss of generality, the z direction. Furthermore, let the system be finite in a direction perpendicular to the stacking direction, e.g., the x direction. Generically, each of the 2D TI ribbons will have topologically protected edge states inside the bulk energy gap with an edge Kramers doublet at a TRI point [19,20]. Let us first inspect the case where the layers are completely decoupled and the band structure of the system does not disperse in the k_z direction. Thus the Kramers doublet of the 1D BZ of the layers become perfectly flat line degeneracies, more precisely Dirac lines, in the surface BZ of the stack. With this stacking procedure we have constructed a weak topological insulator with $\mathbb{Z}_2$ indices $(\nu_0;\nu_1\nu_2\nu_3) = (0;001)$ [8,9], and with Dirac lines instead of Dirac points on its surfaces. This is not surprising, since the stack of 2D TIs is still an effectively 2D system. Generally, one would expect the Dirac lines to break up and leave only Dirac points at TRI momenta once an arbitrary time-reversal interlayer coupling is introduced. This, in turn, leads to a typical surface band dispersion of a weak TI with an even number of surface Dirac cones [8]. However, in the following, we will show that this is not necessarily the case and that the presence of in-plane time-reversal invariance leads to

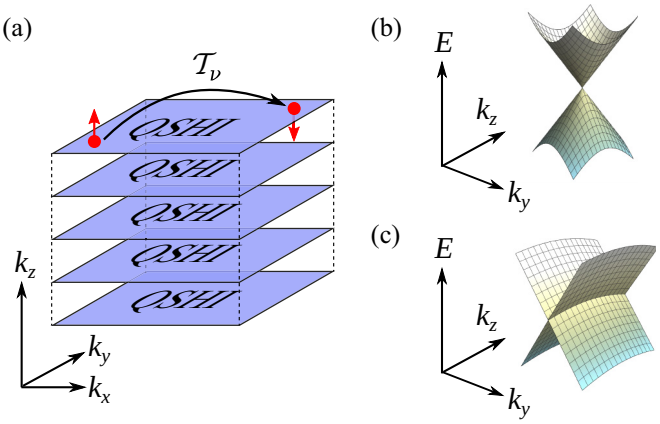

FIG. 1. (Color online) (a) Illustration of the in-plane time-reversal operator $\mathcal{T}_\nu$ in momentum space: the operator flips the spin of an electron and reverses the momentum component parallel to the plane defined by the weak indices $\nu = (\nu_1,\nu_2,\nu_3)$. As demonstrated, a weak TI with $\mathcal{T}_\nu$ symmetry yields a QSHI for any fixed k_z which gives rise to topologically protected Dirac edge states associated with each layer. (b) Typical dispersion of a 2D Dirac particle on the surface of a TI. (c) Typical dispersion of a 1D Dirac particle on the surface of a weak TI with $\mathcal{T}_\nu$ symmetry.

topologically protected Dirac lines even in the full 3D system with coupled layers.

In-plane time-reversal invariance is the 2D analog of the *conventional* time-reversal symmetry with respect to a specific plane Π [see Fig. 1(a)]. The corresponding antiunitary operator $\mathcal{T}_\Pi$ acts similarly to its 3D analog except that the momentum component perpendicular to the plane Π remains unchanged. Without loss of generality, we choose the plane to be (001). Then, the in-plane time-reversal operator for spin-$\frac{1}{2}$ particles reads

$$\mathcal{T}_{(001)} := i(\mathbb{1}\otimes s^y)K \quad \text{with} \quad k_x,k_y,k_z \to -k_x,-k_y,k_z. \tag{1}$$

Here, s^y acts on the spin part of the system, where, again without loss of generality, we have chosen z as the quantization axis of spin and the Pauli matrices as a spin representation. The identity matrix $\mathbb{1}$ is in the space spanned by additional degrees of freedom, such as orbital or sublattice. We further denote the matrix part of the operator, without the action on momentum, by $T_{(001)}$. Note that $\mathcal{T}_{(001)}$ has the same operator structure as the conventional time-reversal operator $\mathcal{T}$. Obviously, for a 2D system, $\mathcal{T}_{(001)}$ and $\mathcal{T}$ are identical. If we deal with a weak TI with weak indices $\nu = (\nu_1,\nu_2,\nu_3)$, we denote the in-plane time-reversal operator associated with the (ν_1,ν_2,ν_3) plane by T_ν.

Since both types of time-reversal operators appear to be very similar, one expects the presence of an analog of Kramers theorem for the in-plane time-reversal symmetric system. To establish this, we recall that a time-reversal symmetric system satisfies $TH(k_x,k_y,k_z)T^{-1} = H(-k_x,-k_y,-k_z)$, i.e., the Bloch Hamiltonian commutes with T at TRI points where $(k_x,k_y,k_z) = (-k_x,-k_y,-k_z)$. For particles with half-integer spin, this implies Kramers theorem [6]. For an in-plane time-reversal symmetric system, we have instead

$$T_{(001)}H(k_x,k_y,k_z)T^{-1}_{(001)} = H(-k_x,-k_y,k_z). \tag{2}$$

Hence, for half-integer particles, the energy spectrum must be at least twofold degenerate along *in-plane time-reversal invariant lines* satisfying $(k_x,k_y,k_z) = (-k_x,-k_y,k_z)$. This thus gives rise to *Kramers lines* along which Kramers-like degeneracies are guaranteed and topologically protected by $\mathcal{T}_{(001)}$ invariance. Since this condition includes also the eight TRI points in the BZ, the Kramers lines always connect certain Kramers points in the BZ.

By the bulk-edge correspondence, one generically finds topologically protected Dirac lines on surfaces perpendicular to the stacking direction. The Dirac lines resemble the dispersion of a 1D Dirac particle in a 2D space: along one direction, it shows the typical linear Dirac dispersion whereas the dispersion is linelike in the perpendicular direction. This is illustrated in Fig. 1(c). If $\mathcal{T}_\nu$ is broken without breaking conventional time-reversal symmetry, only degeneracies at the Kramers points in the BZ are still topologically protected. Therefore each Dirac line splits and the associated 1D Dirac particle decays into two 2D Dirac particles.

Precisely for this reason, topologically protected Dirac lines cannot exist in strong TIs. Consider a strong TI with one Dirac point and without any in-plane time-reversal symmetry. It is always possible to reduce the number of Dirac points of a strong TI to one by introducing suitable translational symmetry breaking and surface potential terms. Now choose an arbitrary plane (klm) and establish the corresponding $\mathcal{T}_{klm}$ symmetry. Before that, the single Dirac point of the strong TI must be connected to the bulk continuum along any line that will later become a Kramers line once in-plane time-reversal symmetry has been established. Otherwise, there would be a second Dirac point at the opposite TRI momentum and the system would not be a strong TI. In the process of establishing $\mathcal{T}_{klm}$ symmetry, the "arms" of the Dirac point, therefore, pull down the bulk bands to which they are attached and thereby close the bulk energy gap. Thus the system cannot be an insulator and either becomes a semimetal or a metal. For this reason, the presence of in-plane time-reversal symmetry, which is essential for the appearance of Dirac lines, is not reconcilable with a strong TI. A demonstration of this feature will be explicitly shown in Sec. IV.

There is another appealing point of view that illustrates the connection between in-plane time-reversal symmetry and Dirac lines in weak TIs. For this, we consider a weak TI with weak indices (001) such that the associated stacking direction is the z direction. Furthermore, let us treat k_z in the corresponding Hamiltonian $H(k_x,k_y;k_z)$ as a parameter. If now in-plane time-reversal symmetry $\mathcal{T}_{(001)}$ is present in the weak TI, we have a 2D quantum spin-Hall insulator (QSHI) for any value of the parameter k_z [see Fig. 1(a)]. This can be easily seen. First, this is clearly the case for $k_z = 0$ and $k_z = \pi$ since the system obeys conventional time-reversal symmetry and is topologically nontrivial. However, as we move along k_z the 2D systems always preserve time-reversal symmetry in the 2D sense due to the presence of in-plane time-reversal symmetry in the full 3D system. Moreover, the bulk gap does not close. Therefore we cannot have a topological phase transition and the collection of 2D systems stay in the QSHI phase for all k_z. This also implies that any such 2D QSHI will have topologically protected (spin-filtered) edge states that will form edge Kramers doublets at the TRI momenta of the 1D

BZ. When we now move along k_z, the edge Kramers doublets cannot be broken, which implies the existence of Dirac lines along the in-plane TRI lines in surface BZ of the weak TI.

On top of this, one can associate a "line" of topological invariants with an insulator respecting in-plane time-reversal symmetry. Indeed, for each value of the stacking direction momentum k_z we can define a 2D topological $\mathbb{Z}_2$ invariant $\nu(k_z)$ [20], which cannot change as we move along k_z. Hence the line of topological invariants can only assume two constant values: $\nu(k_z) = 0$ for a trivial insulator, and $\nu(k_z) = 1$ for an in-plane time-reversal invariant weak TI hosting 1D Dirac electrons on its surfaces.

III. STACKED KANE-MELE MODEL

Having established the general consequences of in-plane time reversal invariance, we apply these notions explicitly to stacked Kane-Mele systems. The Kane-Mele model [18,19] is known to be a realization of a 2D TI in certain parameter ranges. It comprises a 2D nearest-neighbor tight-binding model on a honeycomb lattice with additional $\mathcal{T}$-invariant spin-orbit interaction terms, where $\mathcal{T}$ is the *conventional* time-reversal operator (see Ref. [6]). The model is described by the following Hamiltonian [18,19]:

$$\mathcal{H}_{\mathrm{KM}} = t \sum_{\langle \mathbf{i},\mathbf{j}\rangle,\sigma} c^\dagger_{\mathbf{i}\sigma} c_{\mathbf{j}\sigma} + i\lambda_{\mathrm{SO}} \sum_{\langle\langle \mathbf{i},\mathbf{j}\rangle\rangle,\sigma\sigma'} \nu_{\mathbf{ij}}\, c^\dagger_{\mathbf{i}\sigma} s^z_{\sigma\sigma'} c_{\mathbf{j}\sigma'} + i\lambda_{\mathrm{R}} \sum_{\langle \mathbf{i},\mathbf{j}\rangle,\sigma\sigma'} c^\dagger_{\mathbf{i}\sigma} (\mathbf{s}\times\hat{\mathbf{d}}_{\mathbf{ij}})^z_{\sigma\sigma'} c_{\mathbf{j}\sigma'} + \lambda_\nu \sum_{\mathbf{i}\sigma} \xi_{\mathbf{i}}\, c^\dagger_{\mathbf{i}\sigma} c_{\mathbf{i}\sigma},$$

where the notations and coefficients are as in Ref. [19]. We note that the second term describes in-plane $z \to -z$ symmetric spin-orbit coupling (SOC), the third term represents in-plane Rashba SOC, and the third term is a staggered sublattice potential which breaks inversion symmetry in the plane. As usual, we denote the two interpenetrating hexagonal sublattices of the honeycomb lattice as A and B and follow the conventions of Ref. [19].

From this 2D model, we build up a 3D system by stacking the Kane-Mele layers along the z direction. This is done in such a way that corresponding lattice points of the same sublattice but in different layers lie on top of each other (AA stacking). In order to couple the layers, we introduce a nearest-neighbor interlayer hopping term and an interlayer SOC term, leading us to the model Hamiltonian

$$\mathcal{H} = \sum_l \mathcal{H}_{\mathrm{KM},l} + \tau \sum_{\langle l,l'\rangle} \sum_{\mathbf{i}\sigma} c^\dagger_{\mathbf{i}l\sigma} c_{\mathbf{i}l'\sigma} + i\lambda_{\mathrm{SO},\perp} \sum_{\langle l,l'\rangle} \sum_{\mathbf{i}\sigma\sigma'} \mu_{ll'}\, c^\dagger_{\mathbf{i}l\sigma} s^z_{\sigma\sigma'} c_{\mathbf{i}l'\sigma'}, \tag{3}$$

where l indexes the layers, and $\mu_{ll'} = \pm 1$ for $l \gtrless l'$. We note that after a Fourier transformation, the corresponding Bloch Hamiltonian $H(\mathbf{k})$ is a 4×4 matrix that can be expanded in terms of Dirac matrices and their commutators similar to Ref. [19]. Furthermore, these matrices can be written as Kronecker products of Pauli matrices τ^i in sublattice space and Pauli matrices s^i in spin space. In this way, the interlayer terms of the Hamiltonian become

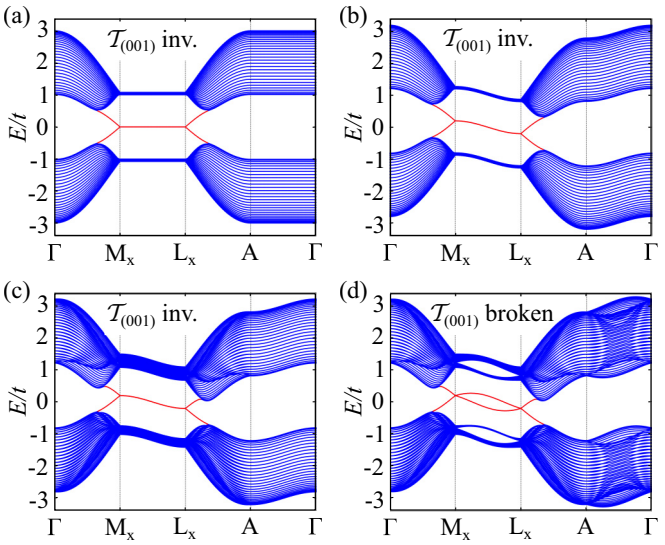

FIG. 2. (Color online) Energy bands for the stacked Kane-Mele model: bands of a (010) slab of width $W = 30$ are shown along high-symmetry lines of the surface BZ for different model parameters (only nonzero parameters are listed in units of t): (a) $\lambda_{\mathrm{SO}} = 0.1$, (b) $\lambda_{\mathrm{SO}} = \tau = 0.1$, (c) $\lambda_{\mathrm{SO}} = \tau = \lambda_{\mathrm{R}} = 0.1$, and (d) $\lambda_{\mathrm{SO}} = \tau = \lambda_{\mathrm{R}} = \lambda_{\mathrm{SO},\perp} = 0.1$. Surface states are highlighted in red. Note the Dirac line in (a)–(c), which is split into two Dirac points in (d) due to the breaking of $\mathcal{T}_{(001)}$ symmetry.

$$H_{ih}(\mathbf{k}) = 2\tau \cos k_z\, (\mathbb{1}\otimes\mathbb{1}), \tag{4}$$

$$H_{\mathrm{SO},\perp}(\mathbf{k}) = -2\lambda_{\mathrm{SO},\perp} \sin k_z\, (\mathbb{1}\otimes s^z), \tag{5}$$

where the interlayer distance has been set to unity. The other terms of the Hamiltonian can be found in Ref. [19]. The relevant in-plane time-reversal operator for this model is $\mathcal{T}_{(001)} = i(\mathbb{1}\otimes s^y)K$ with $(k_x,k_y,k_z) \to (-k_x,-k_y,k_z)$.

In particular, we are interested in surface states which will be studied for a slab of thickness W with (010) surfaces, where W is measured in the number of unit cells. The surface cuts out so-called zigzag edges from each Kane-Mele layer. In other words, we will investigate a stack of infinitely many Kane-Mele layers with zigzag termination. The corresponding Bloch Hamiltonian $H^{(010)}(k_x,k_z)$ of the slab is a $4W\times 4W$ matrix whose energies are obtained by exact diagonalization.

In Fig. 2, the band structure of the (010) Kane-Mele slab along high-symmetry lines of the surface BZ is shown for different model parameters. Here, we ignore the sublattice potential term in H_{KM}. The effect of this term will be discussed at the end of this section. In addition, in Fig. 3, we also plot the corresponding bulk energy bands along high symmetry lines of the bulk BZ.

In Fig. 2(a), only the in-plane hopping and in-plane SOC are nonzero. For the chosen parameters, the bulk spectrum exhibits an energy gap and we find surface states traversing the bulk gap. The band structure along $\overline{\Gamma M_x}$ and $\overline{L_x A}$ is identical to that of the 2D Kane-Mele model with zigzag edges and the same parameter values (see Ref. [21]). For each surface, there is one spin-filtered surface band emerging from the bulk. The bands meet at the TRI momenta M_x and L_x, respectively, where we

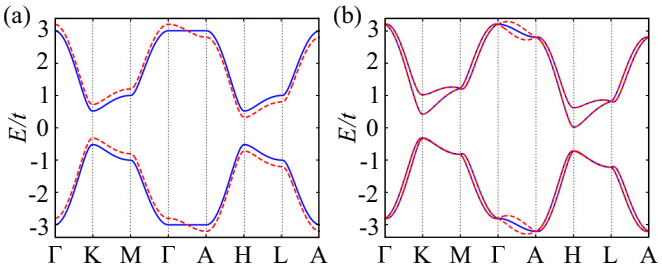

FIG. 3. (Color online) Bulk energy bands for the stacked Kane-Mele model along high symmetry lines of the BZ for different model parameters (only nonzero parameters are listed in units of t): (a) with inversion symmetry: $\lambda_{SO} = 0.1$ (solid blue lines), $\lambda_{SO} = \tau = 0.1$ (dashed red lines); (b) broken inversion symmetry: $\lambda_{SO} = \tau = \lambda_R = 0.1$ (solid blue lines), $\lambda_{SO} = \tau = \lambda_R = \lambda_{SO,\perp} = 0.1$ (dashed red lines).

find twofold Kramers degeneracies, which are topologically protected by conventional time-reversal symmetry. Along $\overline{M_x L_x}$, we find a twofold line degeneracy of the topological bands: a Dirac line. This is easily explained in the light of in-plane time-reversal symmetry. With the chosen parameters, the 2D Kane-Mele model is a topological insulator with a Dirac point at the M_x point of the surface BZ for the zigzag termination. Therefore a stack of these systems forms a weak TI with $\mathbb{Z}_2$ indices $(\nu_0; \nu_1\nu_2\nu_3) = (0; 001)$. Since $\mathcal{T}$ symmetry is preserved for the individual layers and the layers are not coupled, in-plane time-reversal symmetry $\mathcal{T}_{(001)}$ is automatically conserved for the stacked system and we must find topologically protected Dirac lines. The flatness of the Dirac line is due to the absence of dispersion along the k_z direction.

In Figs. 2(b)–2(d), different terms have been added to the Hamiltonian of the system one after the other. In Fig. 2(b), interlayer hopping has been included, which causes the band structure to disperse in the k_z direction. The bands, in particular the Dirac line, acquire a $\cos k_z$ dispersion since the interlayer hopping connects only adjacent layers. However, it is easy to check that the term preserves $\mathcal{T}_{(001)}$ symmetry. Therefore the Dirac line is topologically protected and we have found a fully 3D system that exhibits a 1D Dirac particle on its surface.

It is worth mentioning that the bands of the bulk spectrum [see Fig. 3(a)] are twofold degenerate in the entire BZ due to simultaneous conventional time-reversal and inversion symmetry. For the surface bands of the slab, however, those symmetries only imply that corresponding topological surface bands on *both* surfaces are degenerate. For line degeneracies on just *one* surface, in-plane time-reversal symmetry is essential as can be easily seen by adding an inversion-symmetry breaking term, e.g., in-plane Rashba SOC [see Fig. 2(c)]. It preserves in-plane time-reversal symmetry but breaks inversion symmetry as well as the remaining $\mathcal{U}(1)$ spin symmetry. Hence, in the bulk spectrum, the twofold degeneracies are lifted except at the Kramers points and along the Kramers lines [see Fig. 3(b)]. Furthermore, in the band structure of the slab, the Dirac line is not lifted as shown in Fig. 2(c). An interlayer SOC, however, breaks in-plane time reversal symmetry, while preserving its conventional counterpart, and we see that the effectively 1D Dirac particle decays into two

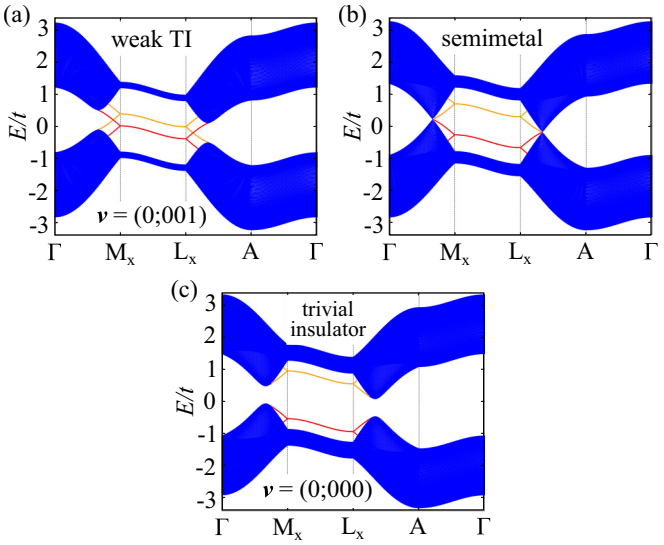

FIG. 4. (Color online) Energy bands for the stacked Kane-Mele model with $\mathcal{T}_{(001)}$ invariance: bands of a (010) slab of width $W = 80$ are shown along high symmetry lines of the surface BZ for different values of the mass term (in units of t): (a) $\lambda_v = 0.2$, (b) $\lambda_v = 0.52$, and (c) $\lambda_v = 0.8$. The mass term does not break in-plane time-reversal invariance with respect to the xy plane. The only other nonzero model parameters are $\lambda_{SO} = \tau = 0.1t$. Surface states are highlighted in red (left surface) and orange (right surface). Note the transition from a weak TI to a trivial insulator at $\lambda_v = 0.52$.

2D Dirac particles, one at the M_x point and the other at the L_x point of the surface BZ with a small shift in energy [see Fig. 2(d)].

So far, we have ignored the staggered sublattice potential term in H_{KM}. However, it is well-known that such a mass term can result in a transition from a topological to a trivial insulator in the 2D Kane-Mele model by closing and reopening the bulk energy gap [18,19]. What happens to the Dirac line in the stacked system if we increase the mass? First of all, it is easy to check that the mass term preserves the relevant in-plane time-reversal symmetry. Therefore the Dirac line cannot be destroyed in the process. However, how can the surface states then be trivial in the trivial sector? The key is the closing of the bulk energy gap. Before, the surface states are connected to both the upper and the lower bulk continuum. However, the process of closing and reopening the gap allows them to merge only with the upper *or* the lower bulk continuum, respectively. In this way, the Dirac line remains intact but the surface states do no longer traverse the bulk energy gap and are, therefore, topologically trivial (see Fig. 4).

IV. CUBIC LIU-QI-ZHANG MODEL

Let us now study in-plane time-reversal invariance in the context of another, more involved model, namely the cubic Liu-Qi-Zhang Hamiltonian [16]. It is derived from a model introduced by Zhang *et al.* [14], which has been succesfully used to describe the Bi_2 Se_3 family of strong topological insulators. It is a 3D nearest-neighbor tight-binding model on a simple cubic lattice with two orbital and two spin degrees of freedom per site. The corresponding Hamiltonian

in momentum representation is [16]

$$\mathcal{H} = \sum_{\mathbf{k}} \sum_{a,b=1}^{2} \sum_{\sigma\sigma'} H_{a\sigma,b\sigma'}(\mathbf{k})\, d^{\dagger}_{\mathbf{k}a\sigma} d_{\mathbf{k}b\sigma'}, \tag{6}$$

with the 4×4 Bloch Hamiltonian [16]

$$H(\mathbf{k}) = \left[M_0 + 6B - 2B \sum_{i=1}^{3} \cos k_i \right] \Gamma_5 + A \sum_{i=1}^{3} \Gamma_i \sin k_i . \tag{7}$$

Here, Γ_j denotes the Dirac matrices of Ref. [16], where also the introduced parameters and notations are explained. We note that the Dirac matrices are Kronecker products of Pauli matrices s^i in spin space and Pauli matrices σ^i in orbital space. The coordinate system used is aligned with the edges of the cubic unit cell and we write $\mathbf{k} = (k_1,k_2,k_3) \equiv (k_x,k_y,k_z)$. The model describes a trivial insulator for $M_0 > 0$ and $M_0 < -12$, a strong TI with $\mathbb{Z}_2$ indices $(1;000)$ or $(1;111)$ for $0 > M_0 > -4B$ or $-8B > M_0 > -12B$, and a weak TI with $\mathbb{Z}_2$ indices $(0;111)$ for $-4B > M_0 > -8B$ [16], where in all cases we have $A = B$. In particular, we focus on the weak TI phase $(0;111)$. For this setup, surface states are studied for a slab of thickness W with (001) surfaces. The corresponding Bloch Hamiltonian, we have to work with, is $4W \times 4W$ and the band structures in the slab geometry are obtained by exact diagonalization.

Let us first check the weak TI phase for in-plane time-reversal invariance with respect to the yz plane. The corresponding operator is

$$\mathcal{T}_{(100)} = i(s^y \otimes \mathbb{1})K \quad \text{with} \quad k_y,k_z \to -k_y,-k_z. \tag{8}$$

It is easy to verify that this symmetry is broken due to the $A \sin k_x\, \Gamma_1$ term in Eq. (7). In Fig. 5, we show what happens to the band structure of the systems in a (001) slab geometry, if we tune the symmetry-breaking term to zero. Obviously, the twofold degeneracy for the surface states along $\overline{\Gamma X}$ ($\overline{YM}$ is not shown) is restored. However, along this line the surface states were connected to the bulk before carrying out the deformation. For this reason, they pull the bulk bands down, resulting in a closing of the bulk energy gap. Hence, the system undergoes a semimetal transition, if we reestablish the in-plane time-reversal symmetry with respect to the yz plane. Besides, this would have happened also for the xz and the xy plane (not shown).

Nevertheless, by analogy with the stacked Kane-Mele model we expect the weak TI with $(0;111)$ to develop Dirac lines without a semimetal transition, if we restore the in-plane time-reversal symmetry with respect to the (111) plane—the plane described by the weak indices. For convenience, we choose a different unit cell with a different coordinate system attached to it. Since a weak TI with weak indices (111) is topologically equivalent to a stack of 2D TIs stacked along the (111) direction, we are going to construct the new unit cell in this light (see Fig. 6).

The Z axis of the new coordinate system points along the (111) direction of the original coordinate system. We further want to align the c axis of the new unit cell with the new Z axis.

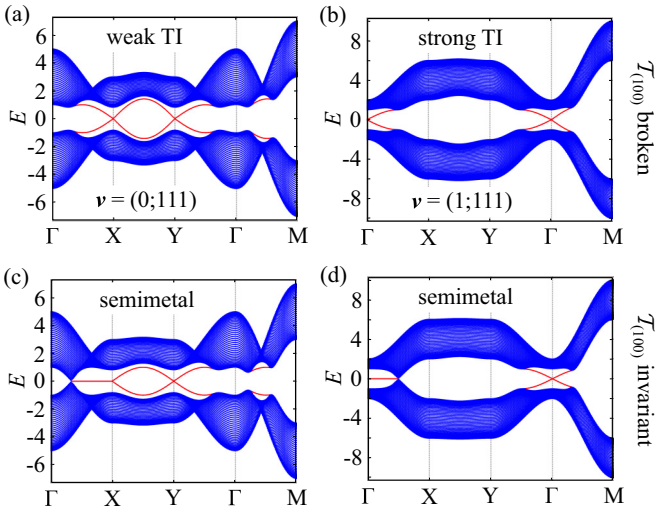

FIG. 5. (Color online) Energy bands for the cubic Liu-Qi-Zhang model: bands of a (001) slab of width $W = 40$ are shown along high symmetry lines of the surface BZ associated with the original cubic unit cell. The model parameters are $M_0 = -5.0$, $A = B = 1.0$ for (a) and (c), and $M_0 = -2.0$, $A = B = 1.0$ for (b) and (d). We show the band structures for broken (upper panels) and restored (lower panels) in-plane time-reversal symmetry with respect to the yz plane. Surface states are highlighted in red.

It turns out that the cubic lattice is best described, in this way, by a hexagonal unit cell with a basis comprising three elements. The primitive lattice vectors of the new unit cell are $\mathbf{a}_1 = a(1,-1,0)$, $\mathbf{a}_2 = a(0,1,-1)$, and $\mathbf{c} = a(1,1,1)$ with respect to the original coordinate system, and $\mathbf{a}_1 = \sqrt{2}a(1,0,0)$, $\mathbf{a}_2 = \sqrt{2}a(-1,\sqrt{3},0)$, and $\mathbf{c} = a(0,0,1)$ with respect to the new rotated coordinates. The elements of the basis lie in different planes, where corresponding adjacent points are relatively shifted by a vector $\Delta = 1/3\,(-\mathbf{a}_1 + \mathbf{a}_2 + \mathbf{c})$.

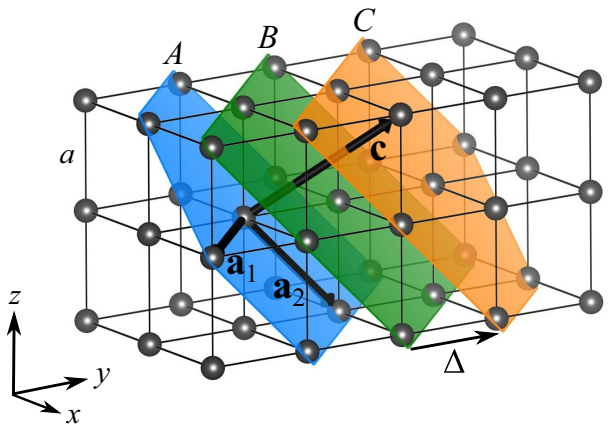

FIG. 6. (Color online) Alternative description of the lattice in the cubic Liu-Qi-Zhang model: the three inequivalent layers corresponding to different elements A,B,C of the new hexagonal unit cell are illustrated. Within the layers, the hexagonal structure of the basal plane is clearly visible. Moreover, the new primitive lattice vectors $\mathbf{a}_1,\mathbf{a}_2,\mathbf{c}$, and the shift vector Δ are shown.

After a Fourier transformation of (6) to real space, the model parameters can be translated to the new coordinate system. Another Fourier transformation back to momentum space then yields a new Bloch Hamiltonian $\tilde{H}(\mathbf{k})$, which is a 12×12 matrix due to the additional sublattice degrees of freedom m,m'. Here, m,m' can assume the values A,B,C. As in Ref. [16], the spin parts and the orbital parts can be expanded in terms of Γ matrices. In addition, the sublattice part can be expanded in 3×3 Gell-Mann matrices [22] λ_i and the corresponding unit matrix denoted by I. The components of the crystal momentum $\mathbf{k}$ are now k_X,k_Y,k_Z with respect to the rotated coordinates. With this, the explicit structure of the Bloch Hamiltonian is

$$\tilde{H} = \tilde{H}_0 \otimes \Gamma_5 + \frac{A}{2} \sum_{i=1}^{3} \tilde{H}_i \otimes \Gamma_i, \tag{9}$$

with

$$\begin{aligned} \tilde{H}_0 = {} & (M_0 + 6B)I - B(2\cos\tilde{X} + \cos\tilde{Y})(\lambda_1 + \lambda_6) \\ & + B \sin\tilde{Y}(\lambda_2 + \lambda_7) \\ & - 2B \cos\tilde{X} \cos\tilde{Y} \cos\tilde{Z}\, \lambda_4 - B \cos\tilde{Z}\, \lambda_4 \\ & + 2B \cos\tilde{X} \sin\tilde{Y} \cos\tilde{Z}\, \lambda_5 + \underline{B \sin\tilde{Z}\, \lambda_5} \\ & - \underline{2B \cos\tilde{X} \sin\tilde{Y} \sin\tilde{Z}\, \lambda_4} \\ & + \underline{2B \cos\tilde{X} \cos\tilde{Y} \sin\tilde{Z}\, \lambda_5}, \end{aligned} \tag{10}$$

$$\begin{aligned} \tilde{H}_1 = {} & \sin\tilde{X}(\lambda_1 + \lambda_6) - \cos\tilde{X}(\lambda_2 + \lambda_7) \\ & + \cos(\tilde{X} + \tilde{Y}) \cos\tilde{Z}\, \lambda_5 \\ & + \sin(\tilde{X} + \tilde{Y}) \cos\tilde{Z}\, \lambda_4 \\ & - \underline{\sin(\tilde{X} + \tilde{Y}) \sin\tilde{Z}\, \lambda_5} \\ & + \underline{\cos(\tilde{X} + \tilde{Y}) \sin\tilde{Z}\, \lambda_4}, \end{aligned} \tag{11}$$

$$\begin{aligned} \tilde{H}_2 = {} & -\sin\tilde{X}(\lambda_1 + \lambda_6) - \cos\tilde{X}(\lambda_2 + \lambda_7) \\ & + \cos(-\tilde{X} + \tilde{Y}) \cos\tilde{Z}\, \lambda_5 \\ & + \sin(-\tilde{X} + \tilde{Y}) \cos\tilde{Z}\, \lambda_4 \\ & - \underline{\sin(-\tilde{X} + \tilde{Y}) \sin\tilde{Z}\, \lambda_5} \\ & + \underline{\cos(-\tilde{X} + \tilde{Y}) \sin\tilde{Z}\, \lambda_4}, \end{aligned} \tag{12}$$

$$\begin{aligned} \tilde{H}_3 = {} & \sin\tilde{X}(\lambda_1 + \lambda_6) - \cos\tilde{X}(\lambda_2 + \lambda_7) \\ & + \cos\tilde{Z}\, \lambda_5 + \underline{\sin\tilde{Z}\, \lambda_4}, \end{aligned} \tag{13}$$

where we have used the notations $\tilde{X} \equiv k_X a/\sqrt{2}$, $\tilde{Y} \equiv k_Y a\sqrt{3/2}$, and $\tilde{Z} \equiv k_Z a\sqrt{3}$. Here, a denotes the lattice constant of the original cubic unit cell. The underlined terms break in-plane time-reversal symmetry with respect to the XY plane.

In the following, everything is expressed in terms of the new coordinate system. The weak indices are now (001). Therefore we are particularly interested in the in-plane time-reversal symmetry with respect to the (001) plane. The associated operator reads

$$\mathcal{T}_{(001)} = i(I \otimes s^y \otimes \mathbb{1})K \quad \text{with} \quad k_X,k_Y \to -k_X,-k_Y, \tag{14}$$

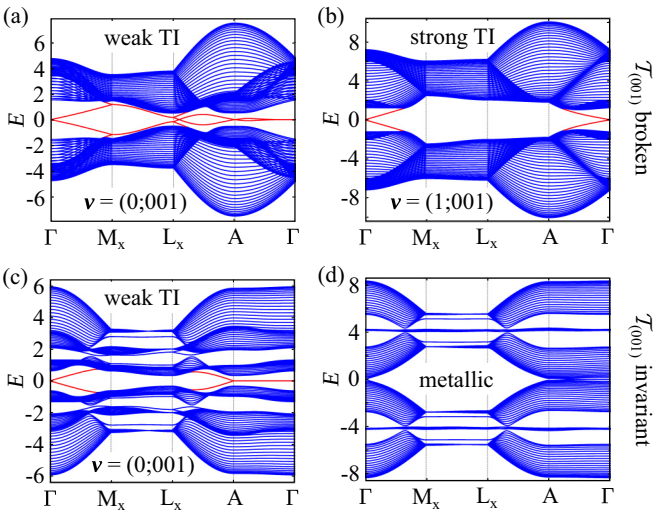

FIG. 7. (Color online) Energy bands for the cubic Liu-Qi-Zhang model: bands of a (010) slab (with respect to the rotated coordinate system) of width $W = 20$ are shown along high-symmetry lines of the surface BZ associated with the hexagonal unit cell. The model parameters are $M_0 = -4.5$, $A = B = 1.0$ for (a) and (c), and $M_0 = -2.0$, $A = B = 1.0$ for (b) and (d). We show the band structures for broken (upper panels) and restored (lower panels) in-plane time-reversal symmetry with respect to the XY plane. Relevant surface states are highlighted in red.

where I denotes the 3×3 unit matrix in sublattice space associated with the three-component basis of the lattice.

We will now study surface states for a slab of thickness W with (010) surfaces. For this, we have to work with a $12W \times 12W$ Bloch Hamiltonian $\tilde{H}^{(010)}(k_X,k_Z)$. The band structures in the slab geometry are again obtained by exact diagonalization.

Let us first have a look at the case, where this symmetry is broken. In Fig. 7(a), we show the band structure in a (010) slab geometry along high symmetry lines of the surface BZ associated with the new unit cell. We find a Dirac point at A, another one at Γ, and two line degeneracies along $\overline{M_x L_x}$. However, these line degeneracies come in pairs and could be easily pushed out of the bulk energy gap. For this reason, they are trivial surface bands. This is also reflected in the fact that in-plane time-reversal symmetry is broken and therefore, they are not topologically protected.

In Eq. (13), all terms of the Bloch Hamiltonian that break in-plane time-reversal symmetry are underlined. We choose to tune *all* k_Z dependent terms to zero except the $\cos k_Z\, \lambda_5 \otimes \Gamma_3$ term, which preserves in-plane TR symmetry. This is possible without closing the bulk energy gap, so the system stays in the weak TI phase. The effect is shown in Fig. 7(c). We observe that the trivial line degeneracies along $\overline{M_x L_x}$ are pushed out of the bulk energy gap. Along the other trivial direction $\overline{A\Gamma}$, a Dirac line forms, which is now topologically protected by in-plane time-reversal symmetry. This is in perfect agreement with the previous observations for the stacked Kane-Mele model.

Out of curiosity, we also ask what happens for the strong TI phase, if we establish in-plane time-reversal symmetry. This is shown in Figs. 5(b) and 5(d) for $\mathcal{T}_{(100)}$ symmetry with respect to the original coordinate system, and in Figs. 7(b) and

7(d) for $\mathcal{T}_{(001)}$ symmetry with respect to the rotated coordinate system. Without the symmetry, in both cases we find one Dirac point at the Γ point of the surface BZ. However, once we restore the considered in-plane time-reversal symmetry, the bulk energy gap closes. As already pointed out at the end of Sec. II, this is due to the connection of the surface states to the bulk continuum. It causes the bulk bands to be pulled down along $\overline{\Gamma X}$ or $\overline{A\Gamma}$, respectively. Therefore it is not possible for strong TIs to have topologically protected Dirac lines.

V. CONCLUSIONS

We have shown how effectively 1D Dirac electrons appear on the surface of weak TIs in the presence of in-plane time-reversal invariance. One might actually view such an in-plane time-reversal invariant weak TI as a collection of 2D QSHIs in momentum space, where the momentum component perpendicular to the surface described by the weak indices serves as a parameter. Topologically protected 1D Dirac electrons cannot appear on the surface of strong TIs. Experimentally, the surface Dirac lines connecting two time-reversal invariant points in an in-plane time-reversal invariant weak TI can, in principle, be detected by angle-resolved photoemission spectroscopy.

ACKNOWLEDGMENT

We thank K. Koepernik, M. Richter, and F. Kirtschig for helpful discussions.

[1] X.-L. Qi and S.-C. Zhang, Rev. Mod. Phys. **83**, 1057 (2011).
[2] L. Fu, Phys. Rev. Lett. **106**, 106802 (2011).
[3] A. Lau and C. Timm, Phys. Rev. B **88**, 165402 (2013).
[4] A. Lau and C. Timm, Phys. Rev. B **90**, 024517 (2014).
[5] A. Alexandradinata, C. Fang, M. J. Gilbert, and A. Bernevig, Phys. Rev. Lett. **113**, 116403 (2014).
[6] M. Z. Hasan and C. L. Kane, Rev. Mod. Phys. **82**, 3045 (2010).
[7] J. E. Moore, Nature (London) **464**, 194 (2010).
[8] L. Fu, C. L. Kane, and E. J. Mele, Phys. Rev. Lett. **98**, 106803 (2007).
[9] L. Fu and C. L. Kane, Phys. Rev. B **76**, 045302 (2007).
[10] B. A. Bernevig, T. L. Hughes, and S. C. Zhang, Science **314**, 1757 (2006).
[11] M. König, S. Wiedemann, C. Brüne, A. Roth, H. Buhmann, L. W. Molenkamp, X.-L. Qi, and S.-C. Zhang, Science **318**, 766 (2007).
[12] D. Hsieh, Y. Xia, L. Wray, D. Qian, A. Pal, J. H. Dil, J. Osterwalder, F. Meier, G. Bihlmayer, C. L. Kane, Y. S. Hor, R. J. Cava, and M. Z. Hasan, Science **323**, 919 (2009).
[13] Y. L. Chen, J. G. Analytis, J.-H. Chu, Z. K. Liu, S.-K. Mo, X. L. Qi, H. J. Zhang, D. H. Lu, X. Dai, S. C. Zhang, I. R. Fisher, Z. Hussain, and Z.-X. Shen, Science **325**, 178 (2009).
[14] H. Zhang, C. Liu, X. Qi, X. Dai, Z. Fang, and S. Zhang, Nat. Phys. **5**, 438 (2009).
[15] B. Rasche, A. Isaeva, M. Ruck, S. Borisenko, V. Zabolotnyy, B. Büchner, K. Koepernik, C. Ortix, M. Richter, and J. van den Brink, Nat. Mater. **12**, 422 (2013).
[16] C.-X. Liu, X.-L. Qi, and S.-C. Zhang, Physica E **44**, 906 (2012).
[17] Q. D. Gibson, D. Evtushinsky, A. N. Yaresko, V. B. Zabolotnyy, M. N. Ali, M. K. Fuccillo, J. Van den Brink, B. Büchner, R. J. Cava, and S. V. Borisenko, Sci. Rep. **4**, 5168 (2014).
[18] C. L. Kane and E. J. Mele, Phys. Rev. Lett. **95**, 226801 (2005).
[19] C. L. Kane and E. J. Mele, Phys. Rev. Lett. **95**, 146802 (2005).
[20] L. Fu and C. L. Kane, Phys. Rev. B **74**, 195312 (2006).
[21] L. Cano-Cortés, C. Ortix, and J. van den Brink, Phys. Rev. Lett. **111**, 146801 (2013).
[22] B. Li, Z.-H. Yu, and S.-M. Fei, Sci. Rep. **3**, 2594 (2013).